International Journal of Applied Earth Observations and Geoinformation 113 (2022) 102999

Contents lists available at ScienceDirect

International Journal of Applied Earth Observation and Geoinformation

journal homepage: www.elsevier.com/locate/jag

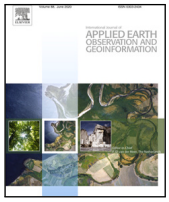

Benchmarking laser scanning and terrestrial photogrammetry to extract forest inventory parameters in a complex temperate forest

Daniel Kükenbrink *, Mauro Marty, Ruedi Bösch, Christian Ginzler

Swiss Federal Institute for Forest, Snow and Landscape Research WSL, Zurichstrasse 111, Birmensdorf, 8903, Switzerland

ARTICLE INFO

Keywords:
Terrestrial laser scanning
Mobile laser scanning
Unmanned aerial vehicle laser scanning
Terrestrial photogrammetry
Structure from motion
Forest inventory
3D point cloud
LiDAR

ABSTRACT

National forest inventories (NFI) are important for the assessment of the state and development of forests. Traditional NFIs often rely on statistical sampling approaches as well as expert assessment which may suffer from observer bias and may lack robustness for time series analysis. Over the course of the last decade, close-range remote sensing techniques such as terrestrial and mobile laser scanning became ever more established for the assessment of three-dimensional (3D) forest structure. With the ongoing trend to make the systems smaller, easier to use and more efficient, the pathway is being opened for an operational inclusion of such devices within the framework of an NFI to support the traditional field assessment. Close-range remote sensing could potentially speed up field inventory work as well as increase the area in which certain parameters are assessed. Benchmarks are needed to evaluate the performance of different close-range remote sensing devices and approaches, both in terms of efficiency as well as accuracy. In this study we evaluate the performance of two terrestrial (TLS), one handheld mobile (PLS) and two drone based (UAVLS) laser scanning systems to detect trees and extract the diameter at breast height (DBH) in three plots with a steep gradient in tree and understorey vegetation density. As a novelty, we also tested the acquisition of 3D point-clouds using a low-cost action camera (GoPro) in conjunction with the Structure from Motion (SfM) technique and compared its performance with those of the more costly LiDAR devices. Among the many parameters evaluated in traditional NFIs, the focus of the performance evaluation of this study is set on the automatic tree detection and DBH extraction.

The results showed that TLS delivers the highest tree detection rate (TDR) of up to 94.6% under leaf-off and up to 82% under leaf-on conditions and a relative RMSE (rRMSE) for the DBH extraction between 2.5 and 9%, depending on the undergrowth complexity. The tested PLS system (leaf-on) achieved a TDR of up to 80% with an rRMSE between 3.7 and 5.8%. The tested UAVLS systems showed lowest TDR of less than 77% under leaf-off and less than 37% under leaf-on conditions. The novel GoPro approach achieved a TDR of up to 53% under leaf-on conditions. The reduced TDR can be explained by the reduced area coverage due to the chosen circular acquisition path taken with the GoPro approach. The DBH extraction performance on the other hand is comparable to those of the LiDAR devices with an rRMSE between 2 and 9%.

Further benchmarks are needed in order to fully assess the applicability of these systems in the framework of an NFI. Especially the robustness under varying forest conditions (seasonality) and over a broader range of forest types and canopy structure has to be evaluated.

1. Introduction

National forest inventories (NFI) are an important framework for the assessment of the current state and development of forests as well as their management. Traditional NFIs are labor intensive and costly and often rely on statistical sampling approaches. Additionally, many relevant forest variables are collected by expert assessment (e.g. canopy cover and layering), which are subject to observer bias. Possibilities to switch from an expert assessment to a more quantitative measurement are therefore sought after. Advances in the field of close-range remote sensing over the past years introduced promising opportunities for supporting NFIs in order to increase the area under investigation and to switch from an expert assessment to a more quantitative, reproducible and robust measurement of selected forest inventory parameters. Most recent studies on the use of close-range remote sensing for NFI as well as this study focus on the extraction of tree parameters (position, diameter at breast height (DBH), tree height etc.) (e.g. Mokroš et al.,

* Corresponding author.
E-mail address: daniel.kuekenbrink@wsl.ch (D. Kükenbrink).

https://doi.org/10.1016/j.jag.2022.102999
Received 11 March 2022; Received in revised form 15 August 2022; Accepted 22 August 2022
Available online 5 September 2022

Table 1
Key parameters of analyzed three plots (FP05, FP07, FP08). The number of trees for the three diameter classes analyzed in this study are reported with DBH thresholds of 7, 12 and 20 cm. Further, the average distance to the closest neighboring tree for all trees with a DBH < 12 cm is reported to further quantify the density of the analyzed plots.

Plot name	# Trees [DBH ≥ 7 cm]	# Trees [DBH ≥ 12 cm]	# Trees [DBH ≥ 20 cm]	Tree density [N/ha]	DBH range [cm]	Avg. DBH [cm]	Avg. Distance to closest tree with DBH < 12 cm [m]	Avg. Slope [°]
FP05	90	83	74	360	7 - 69	31.2	9.47	8.2
FP07	107	63	38	428	7 - 90	23.3	2.23	6.1
FP08	190	79	49	760	7 - 82	18.4	2.13	5.0

2021; Gollob et al., 2020), also due to the availability of accurate reference measurements. However, close-range remote sensing further shows potential to extract inventory relevant parameters where often less accurate reference measurements are available (e.g. forest regeneration assessment (e.g. Heinzel and Ginzler, 2019), detection of dead wood (e.g. Yrttimaa et al., 2019), microhabitat assessment (e.g. Rehush et al., 2018) etc.)

Terrestrial laser scanning (TLS) devices have long been established as the gold standard for acquiring detailed, high resolution and accurate three-dimensional (3D) point clouds in forest environments (Liang et al., 2016). With the ongoing advances in making the originally heavy and complicated devices more user friendly (e.g. weight reduction), TLS instruments have become more and more readily available and accessible. Despite the improvements in terms of size, costs, resolution and speed of TLS instruments, they still suffer from inherent limitations. Multi-station TLS acquisitions suffer from occlusion effects (Abegg et al., 2017; Schneider et al., 2019). These occlusion effects can be partly mitigated by increasing the number of scan positions, at the cost of increasing acquisition times.

The static nature of TLS acquisitions and the problems caused by occlusion inspired efforts to combine the ability to acquire detailed 3D point clouds with a mobile acquisition strategy. In recent years, developments of mobile laser scanning (MLS) devices (Čerňava et al., 2019; Forsman et al., 2016; Kukko et al., 2012; Liang et al., 2014a, 2018) and hand-held personal laser scanners (PLS) (Balenović et al., 2020a) became more relevant. This approach mitigates the inherent limitations of TLS instruments caused by occlusion effects at the cost of reduced resolution and precision. Both MLS and PLS approaches are reliant on the Simultaneous Localization and Mapping (SLAM) technology (Durrant-Whyte and Bailey, 2006) often in combination with an Inertial Measurement Unit (IMU). The SLAM approach allows the application of such a device in environments with weak or no GNSS reception.

The above mentioned LiDAR devices are all restricted to plot- or stand-level assessments. For larger scale 3D forest structure assessments, a shift in observation angle from below canopy to above canopy is needed. Drone-based laser scanning solutions (unmanned aerial vehicle laser scanning, UAVLS) could deliver an interesting compromise between level of detail and area coverage. UAVLS acquisition have shown to successfully complement ground-based TLS acquisition (Schneider et al., 2019; Terryn et al., 2021), assess forest structure (Bruggisser et al., 2019; Morsdorf et al., 2018), as well as acquire forest inventory relevant parameters (e.g. Jaakkola et al., 2017; Liang et al., 2019; Wieser et al., 2017).

Also non-LiDAR devices were used in the context of forest inventory measurements to extract 3D information from forest plots. Piermattei et al. (2019) used terrestrial photogrammetry based on structure from Motion (SfM) for deriving tree positions, DBH and stem curves by means of a single consumer grade camera. The success for extracting a usable 3D point cloud from multiple images is highly dependent on the camera settings, environmental conditions and acquisition pattern chosen by the operator (Piermattei et al., 2019). All these constraints can make the SfM approach cumbersome and prone to failure and hence less favorable in comparison to the above mentioned LiDAR devices. Action cameras, such as the GoPro cameras, could be an interesting and definitely low-cost alternative. The biggest advantage of such a small action camera is the ease of use as well as relatively stable image acquisition under movement with varying lighting conditions. To our best of knowledge, such camera systems have not yet been evaluated for the acquisition of forest inventory metrics.

With these recent technological advances both in terms of sensor development as well as in terms of 3D point cloud assessment, we are steadily stepping towards a more operational use of such close-range remote sensing devices within a NFI. Benchmarks are needed in order to assess the suitability of each device. For a successful and operational implementation of close-range remote sensing, certain key aspects have to be met. First of all, fast and robust data acquisition within seasonal constraints of the specific NFI is key for an operational inclusion. Furthermore, an acquisition approach should be suitable for a majority of forest types and structures with varying degrees of complexity as encountered in the specific country. In this study we evaluate the suitability of 3 ground-based LiDAR devices (two TLS (leaf-off and leaf-on) and one PLS (leaf-on)), two above canopy LiDAR devices (leaf-off and leaf-on) as well as a terrestrial SfM approach using a GoPro action camera (leaf-on). Three complex forest plots with a steep gradient in terms of tree density and understorey vegetation density have been chosen for this benchmark test. Within this study we evaluate the performance of each device in terms of tree detection rate, accuracy in tree position as well as in DBH extraction and the time needed for data acquisition.

2. Study area and data

2.1. Study area and reference data

The study area is located in a temperate mixed forest close to Zurich, Switzerland. Three 50 m × 50 m plots, corresponding to the interpretation area of the Swiss National Forest Inventory (Fischer and Traub, 2019), were defined, representing a gradient in tree density, tree size and structural complexity with varying densities in understorey vegetation. Within these three sample plots, the position, DBH and species of all trees with a DBH > 7 cm were measured. Tree positions were measured with a total station MS50 (Leica Geosystems) using a network of distributed reference points. The measurement of the stem center was conducted at DBH height, adding an offset corresponding to half of the DBH. The network of reference points was surveyed beforehand, based on a total station setup using three measured dGNSS points (3D accuracy ≈ 2 cm), followed by a traverse using multiple backsight positioning (accuracy < 1 cm). The three plots were chosen to have their center point on one such absolutely referenced surveying points each, allowing for subsequent measurements and the establishment of a long term monitoring for subsequent testing of new technologies and methodologies. Due to the definition of the plot centers on these reference points, the three selected plots overlap partially. The plots are hereafter named after the name of the fixed surveying points (i.e. FP05, FP07, FP08). DBH was measured using a traditional caliper in North–South and East–West directions. For trees with a DBH larger than the measurable diameter of the used caliper (80 cm), the circumference was measured using a measuring tape. Table 1 gives an overview of the key parameters of the selected plots. Fig. 1 shows the three plots with marked tree positions including tree species. The dominant tree species are beech (*Fagus sylvatica*) followed by fir (*Abies alba*) and spruce (*Picea abies*).

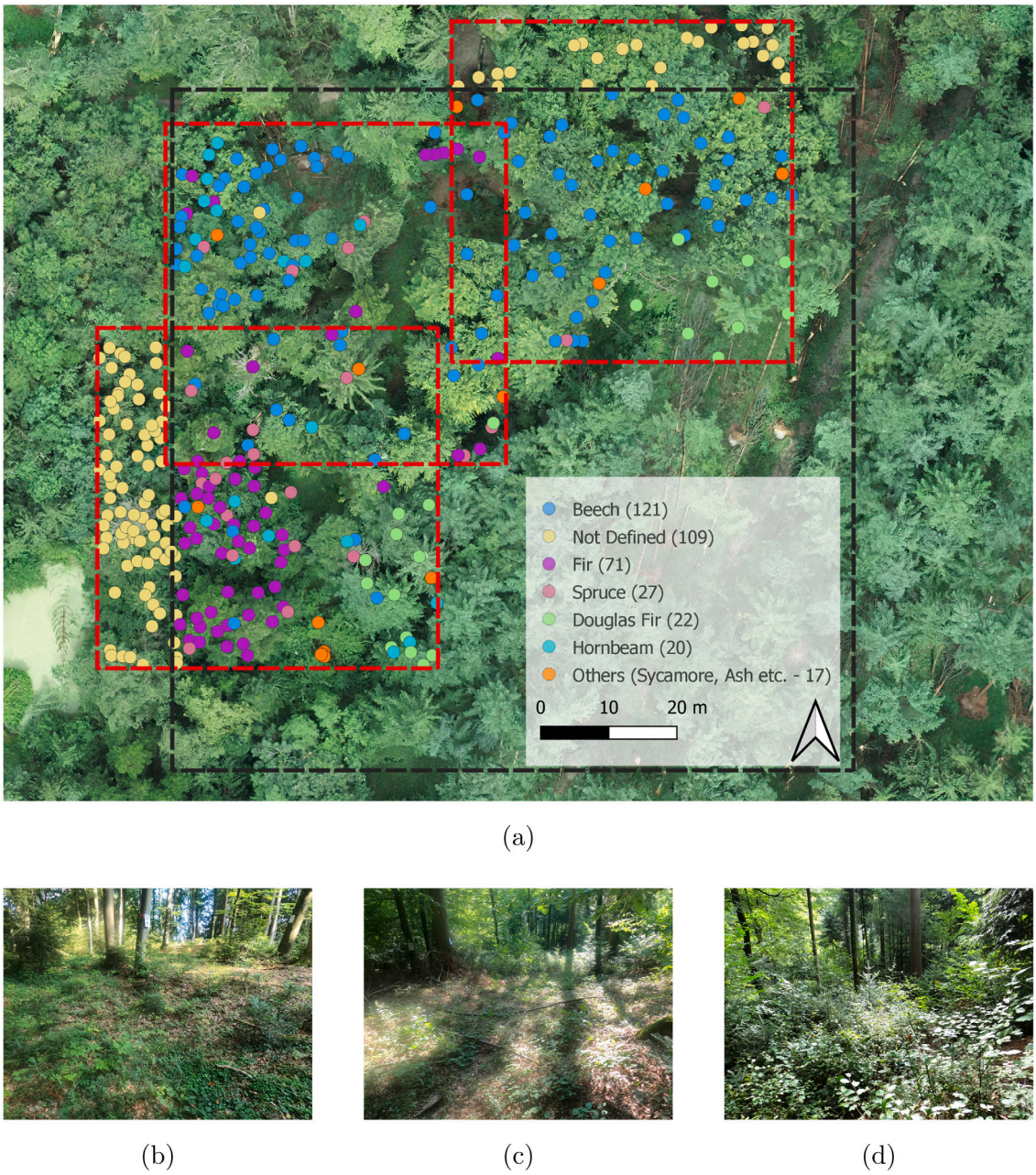

Fig. 1. Study area with designated plots FP05 (northern most plot, photo in 1(b)), FP07 (middle plot, photo in 1(c)), and FP08 (southern most plot, photo in 1(d)). Tree species were only acquired for trees within the larger 1 ha study site marked in black. For trees outside this 1 ha plot, only position and DBH was measured. The orthoimage was acquired using a DJI Phantom 4 RTK in July 2021.

2.2. TLS data

Two TLS campaigns were performed. A FARO Focus 3D S120 phase-shift TLS (henceforth FARO) was used under leaf-off conditions in January 2020 to acquire a reference point cloud with minimal occlusion due to missing foliage (see Table 2 for detailed description of all tested laser scanning devices). The FARO campaign covered a 1 ha area (black dashed square in Fig. 1) including a roughly 5–10 m buffer around it. Spherical targets were used for co-registration of the 125 scan positions with a distance between consecutive positions of approximately 10 m. The acquisition of the entire 1 ha large plot took 6 full working days with two persons. The acquired point clouds were afterwards processed and co-registered in the FARO Scene software suite. The co-registered point cloud was subsequently transformed into the Swiss LV95 (CH1903+, EPSG:2056) coordinates system using spherical targets that were placed onto seven absolutely referenced surveying points distributed over the entire plot area. The resulting transformed point cloud acts as the reference point cloud to which all other acquired point clouds were referenced to.

Another TLS campaign, focusing on the three main 50 m × 50 m plots, was conducted in September 2020 under leaf-on conditions using the time-of-flight TLS instrument Leica BLK360. The Leica BLK360 system convinces through its lightweight (< 1 kg) build and easy-to-use interface (one button). Table 2 gives further details on the tested Leica TLS device. No artificial reference targets were used for the co-registration of scan positions, as the automatic co-registration algorithm provided by the Leica Cyclone software suite (v1.6.2) was used, which aligns overlapping scans by detecting and aligning flat surfaces in the 3D point clouds. To facilitate the automatic alignment,

Table 2
LiDAR systems specifications. * FOV for ground-based sensors as vertical/horizontal. **Foot print size is @ 10 m for ground-based sensors and @ 100 m for UAVLS systems. ***Flight duration correspond to 52 ha for VUX1 and 1 ha for miniVUX2 acquisitions. If no values are given, these are not applicable for the specific sensor or unknown.

	TLS		PLS	UAVLS	
	FARO	Leica	GeoSLAM	Riegl	Riegl
	Focus3D S120	BLK360	ZebRevo	VUX1	miniVUX2
Wavelength [nm]	905	830	905	1550	905
Field of view*	305°/360°	300°/360°	270°/360°	330°	120°
Viewing direction				+/- 5° off-nadir	nadir
Measurement rate [pts/s]	488'000	300'000	43'000	550'000	200'000
Beam divergence [mrad]	0.19	0.4		0.35	1.6 × 0.5
Foot print size** [mm]	5	6.2		50	160 × 50
Accuracy [mm]	2	4	6	10	15
Max range [m]	120	60	30	230	330
Flight height a.g. [m]				100	60
Flight duration [min]***				150	12

the scan positions were chosen to be closer together, compared to the FARO scans, with an approximate distance of 5 m in a gridded pattern. To cover the entire area comprised by the three 50 m × 50 m plots a total of 136 scan positions were used. The Leica BLK360 instruments allows for a relatively fast scanning time (in average 6 min per scan position including relocations and scanning with the highest resolution setting). The automatic alignment in such complex environments is prone to fail, therefore most of the scans had to be aligned manually in a post-processing step using the Leica Cyclone software suite. The total processing time to acquire a co-registered point cloud took around 4 h for each plot. The relatively aligned point clouds were afterwards transformed into absolute coordinates (CH1903+) by matching the point cloud to the absolutely registered point cloud acquired with the FARO scanner. This was performed by a first visual alignment of the two point clouds, followed by a fine registration using the iterative closest point method implemented in CloudCompare (v2.11.3).

2.3. PLS data

The PLS device used in this study was the ZebRevo RT lightweight mobile laser scanner produced by GeoSLAM (GeoSLAM Ltd. Nottingham). The system integrates a rotating 2D scanning device and an IMU. By utilization of the IMU in conjunction with the SLAM technology, the system is able to localize itself in 3D space in GPS challenging environments such as forests. The laser device operates at a wavelength of 905 nm (backscattered intensities are not stored) and has a data acquisition rate of 43200 points per second at a maximum range of 30 m indoors (15–20 m in forest environments). The relative accuracy of the measured points is 2–3 cm in normal light conditions (Nocerino et al., 2017; Cabo et al., 2018) (also see Table 2). The data acquisition path follows a regular grid pattern with approximately 5–10 m between neighboring lines (see Fig. 2(c)). For a successful acquisition it is important to start and end the acquisition at the same point. The SLAM approach of the device tends to add a drift to the trajectory after an acquisition time of 15–20 min. For plot FP08 we had to split the acquisition into two parts as the acquisition time exceeded this maximum threshold. We ensured an overlap between the two acquisitions for a successful alignment of the two scan patterns. The alignment of the two acquisitions as well as the referencing to the FARO point cloud was performed using the same approach as for the alignment of the Leica point-cloud (Section 2.2).

2.4. UAVLS data

Two UAVLS campaigns were conducted using two different scanning devices. A larger campaign covering the entire forest area with 52 ha was acquired during leaf-off conditions in March 2020 using a Riegl VUX1 system mounted on a petrol fueled drone helicopter operated by the company Aeroscout (Aeroscout GmbH, Switzerland). Two flights were conducted following the same trajectory with varying mounting angles of the device (+/−5° off-nadir) in order to add more observation angles to increase canopy penetration. The second campaign was conducted under leaf-on conditions in September 2020 using a Riegl miniVUX2 scanner mounted on a DJI Matrice M600 Pro drone. The acquisition pattern was a regular grid pattern with 20 m side distance, covering the 1 ha large plot including a buffer zone of approximately 20 m to all sides. The flight pattern consists of two rectangular grids rotated by 90°. The rotation by 90° of the second rectangular grid served to increase the observation angle to be able to better penetrate the canopy. Fig. 3 shows the acquisition patterns for both flight campaigns. Table 2 shows the key parameters of the two UAVLS systems. Post flight processing of the measured point cloud for the VUX1 acquisition was performed by the company Aeroscout, resulting in an analysis ready, absolutely registered point cloud (Swiss reference system CH1903+). Post flight processing of the miniVUX acquisition was performed using Pospac 8.5 to correct the flight trajectory (PPK) and the Riegl processing facilities (RiProcess v1.8.7), resulting in an absolutely referenced point cloud (Swiss reference system CH1903+, 3D accuracy < 5 cm). As the processed UAVLS point clouds are already absolutely referenced, no further alignment to the FARO reference point cloud was performed.

2.5. Terrestrial photogrammetry

A GoPro Hero 8 Black action camera was used to acquire several hundreds of overlapping images per plot. The GoPro was mounted on a gimbal to increase stability and reduce motion blur effects. The GoPro was setup to acquire time-lapse photos with an interval of 0.5 s. Lens mode was set to wide which corresponds to a focal length of 16 mm (35 mm focal length equivalent). The GoPro Hero 8 Black has a 12 megapixel sensor. The acquisition pattern was chosen to follow the recommendations by Piermattei et al. (2019), which in theory comprises of three concentric circles plus two linear transects in roughly North–South and East–West directions. The camera was pointed towards the plot center for the two larger concentric circles and towards the plot edge for the small, inner circle. For the East–West and North–South transects, the camera was roughly pointed towards the Southern/Northern and Eastern/Western border of the plot respectively. Fig. 2(d) shows the actual acquisition path for the plot FP05.

Total acquisition time for one plot ranged from 14 to 19 min and resulted in 1730 to 2294 images. For point cloud scaling, artificial markers printed from Agisoft Metashape (v1.6.3) were pinned onto tree trunks distributed over the entire plot. Two markers were printed onto a laminated A4 paper, where the distance between the two markers is exactly known. Alignment of the images was performed using Agisoft Metashape (v1.6.3), following the procedure and suggestions on parameter settings as described in Piermattei et al. (2019). Markers were automatically detected in the images and the scale bars were defined to be able to correctly scale the point cloud. The camera was calibrated

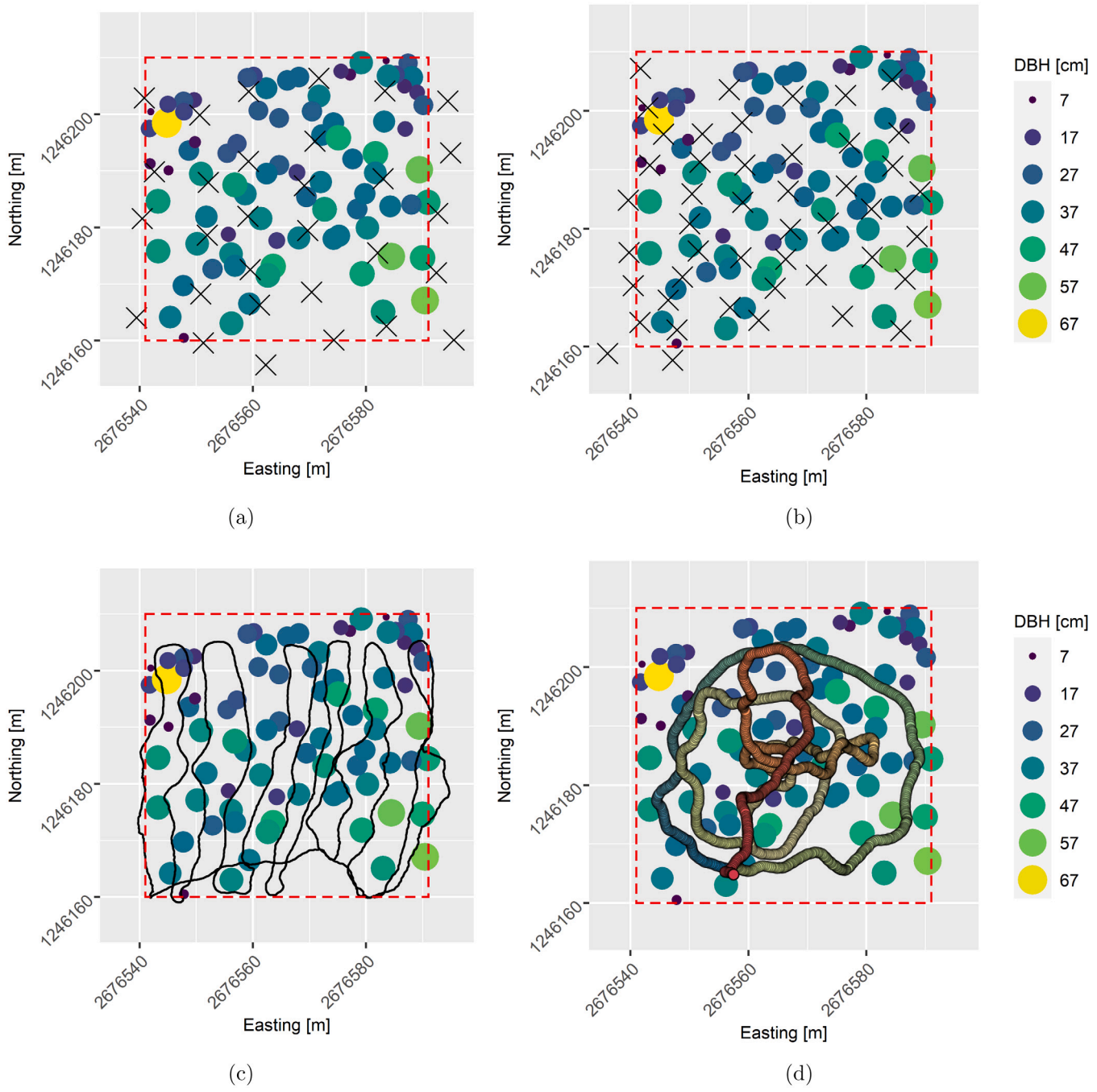

Fig. 2. Different data acquisition patterns for the used ground-based systems: FARO (a), Leica BLK360 (b), GeoSLAM ZebRevo (c), GoPro Hero 8 Black (d). Displayed are only the acquisition patterns for the plot FP05. Scan positions are marked as black crosses. ZebRevo path is shown as a black line. GoPro images are denoted as colored circles, where the color denotes acquisition time (blue = start, red = end). Tree positions are denoted as colored circles where size and color are corresponding to the measured reference measurement. (For interpretation of the references to color in this figure legend, the reader is referred to the web version of this article.)

using the lens calibration feature within Agisoft Metashape. This step is particularly important due to the large distortions within the GoPro images caused by the fish eye lens.

After successful alignment, tie points were filtered to include only those with at least 2 images and low reconstruction uncertainty (< 50) using the gradual selection tool within Agisoft Metashape. Afterwards, camera positions were optimized and the dense point cloud was built with high quality and mild depth filtering. The generated dense point cloud was afterwards filtered by confidence (>3), resulting in the final, not yet correctly rotated point cloud in local coordinates.

The entire processing pipeline was performed on a desktop PC with an Intel Xeon W-2125 4-core processor with 4.01 GHz, 32 GB ram memory and an Nvidia Quadro RTX 4000 GPU. For the registration of the point cloud to the Swiss CH1903+ coordinate system, the same procedure as with the Leica point-cloud (see Section 2.2) was performed. Table 3 gives further details on the SfM acquisition and processing for the three different plots.

3. Methods

3.1. Automatic tree detection & DBH extraction

A pre-requisite for the chosen automatic tree detection and DBH extraction is a height-normalized point cloud. Ground points were

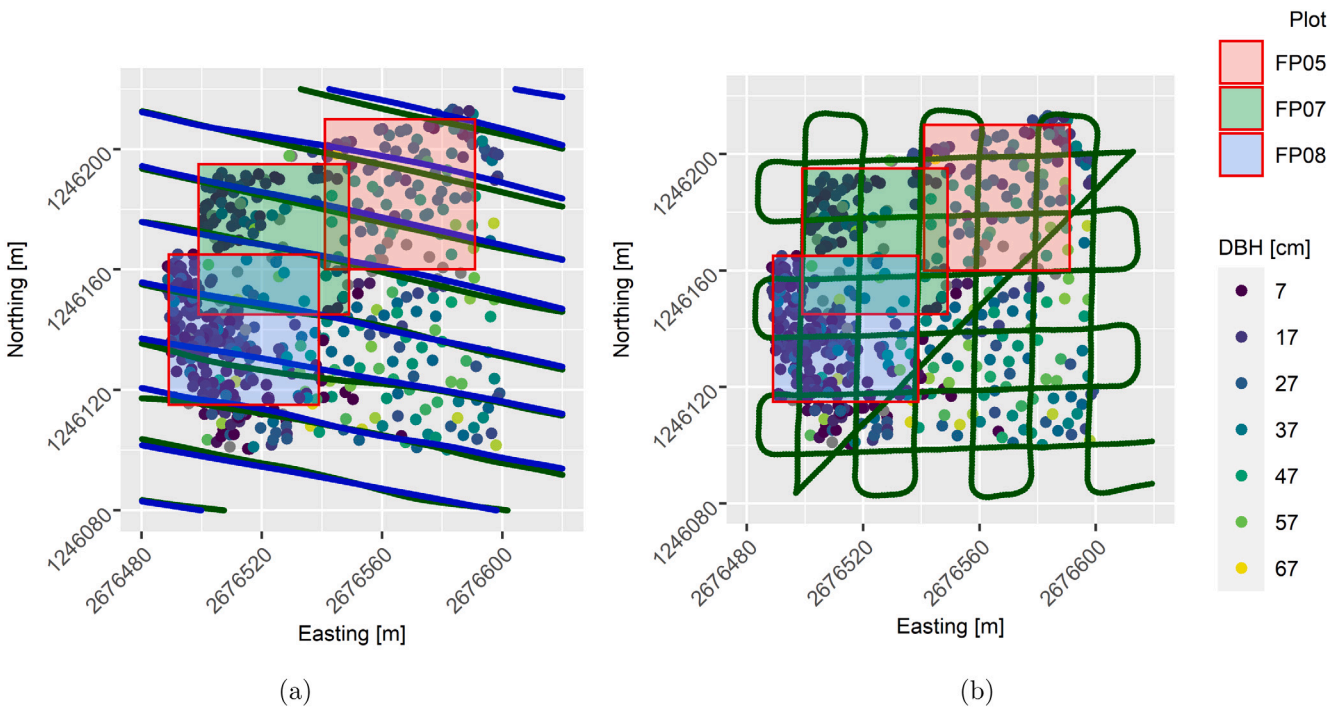

Fig. 3. Acquisition patterns acquired with the VUX1 3(a) and the miniVUX2 3(b) system by Riegl. The VUX1 acquisition was operated and planned by the Swiss company Aeroscout GmbH. Only the part of the acquisition pattern above the 1 ha large study site are shown (entire VUX1 acquisition comprises 52 ha). Tree positions are denoted as colored circles, where color denotes the measured reference DBH. (For interpretation of the references to color in this figure legend, the reader is referred to the web version of this article.)

Table 3
SfM acquisition characteristics with GoPro Hero 8 Black. Alignment time for FP05 and FP07 (marked with a *) is relatively shorter as we enabled sequential reference selection, which can reduce computation time, but often leads to unsuccessful alignment in more complex forest structures. Number of tie and dense points are after applying gradual selection and point cloud filtering by confidence.

	FP05	FP07	FP08
# images	1730	1741	2294
acquisition time [mm:ss]	14:48	15:05	19:47
time image alignment [hh:mm]	1:51*	3:13*	6:05
time dense point cloud [hh:mm]	14:03	13:46	16:53
# tie points (filtered)	852'065	371'711	606'161
# dense points (filtered)	61'765'396	65'699'854	93'961'600

classified for the FARO TLS point cloud using LASTools *lasground* function (Isenburg, 2015). The classified ground points of the FARO TLS point cloud served as the reference ground points used for height normalization for all other point clouds. This was chosen in order to reduce normalization inconsistencies due to different ground definitions from the various point cloud sources (i.e. due to occlusion or reduced coverage). All point clouds were then normalized using LASTools *lasheight* function (Isenburg, 2015) with the *-replace_z* option.

For close-range remote sensing to become an operational support in NFI applications, robust and automatic feature extraction (e.g. tree position, DBH etc.) from the produced point clouds is one of the most important steps. In this study we adapted the existing, freely available TreeLS (de Conto et al., 2017) library written in the statistical programming language R that was developed to extract tree positions and key tree parameters (DBH, height) and is optimized for ground-based instruments (TLS, PLS). One limitation of this package is that it performs less accurate when dense understorey vegetation is present in the plots, often resulting in many falsely detected trees due to shrub or rejuvenation forest. We therefore added multiple filtering steps on the normalized point clouds before applying the tree detection routine. We filtered the point cloud to only extract a vertical slice between 1 and 3 m (1 and 5 m in the case of UAVLS in order to counteract the increased occlusion effects on the lower tree trunks in UAVLS data). For performance reasons, the point clouds were downsampled by randomly selecting a point within a 1 cm large voxel. The verticality geometric feature in a neighborhood of 30 cm was calculated for each point using CloudCompare. This geometric feature (value range between 0 and 1, where 1 is completely vertical) allows us to extract mainly tree trunks and remove most points belonging to understorey vegetation. We excluded all points with a verticality of less than 0.8 (thresholds based on visual inspection on the impact of the filtering). Stem detection was then performed using the *treeMap* function using the knn method to detect circular point cloud clusters within the vertical slice (see de Conto et al. (2017)). Subsequently the detected stem points were denoised using the *stemPoints* function in conjunction with the hough transformation method following the suggestions in de Conto et al. (2017). Final tree position and also the DBH was extracted using the *tlsInventory* function of the TreeLS library, using the RANdom SAmple and Consensus (RANSAC) cylinder fitting.

The excessive point cloud filtering in order to detect tree positions could lead to larger errors in extracted DBH, especially for point clouds of lower resolution. We therefore added a step to improve the DBH estimation by extracting for each initially detected tree a subset of the original, unfiltered point cloud. This subset was defined as a circular cut with the detected tree position as center and the initially estimated DBH as diameter plus a buffer of 9 cm. The vertical extent of this subset was defined to be between 1.1 and 1.5 m. For this subset an additional DBH estimation was performed.

3.2. Performance evaluation

The performance of the automatic tree detection and DBH extraction (Section 3.1) was evaluated using the tree positions and DBH measured during the field inventory (also see Section 2.1). All trees detected in the point clouds were searched for a matching reference tree within the inventory dataset. A detected tree was declared a match if the tree position was less than 1 meter away from the reference tree and the DBH deviation was less than 50% of the reference measurement.

The accuracy of automatic tree detection was evaluated regarding their detection rate (TDR[%]) as well as the amount of falsely detected trees.

$$TDR(\%) = \frac{n_{match}}{n_{ref}} \times 100 \quad (1)$$

where n_{match} is the number of correctly matched reference trees, n_{ref} is the total number of reference trees within the plots.

The accuracy of the automatic DBH extraction was assessed with the root mean square error (RMSE):

$$RMSE = \sqrt{\frac{1}{n_{match}} \sum_{i=1}^{n_{match}} (\widehat{dbh_i} - dbh_i)^2} \quad (2)$$

where $\widehat{dbh_i}$ is the estimated DBH from the point cloud and dbh_i is the measured DBH of the reference acquisition.

Relative RMSE (rRMSE) was calculated with

$$rRMSE = \frac{RMSE}{\overline{dbh}} \times 100 \quad (3)$$

with

$$\overline{dbh} = \frac{1}{n_{match}} \sum_{i=1}^{n_{match}} dbh_i \quad (4)$$

being the average DBH of the reference data.

For reporting on TDR, falsely detected trees and $rRMSE$ we divided the trees in three diameter classes with a minimum DBH of 7 cm, 12 cm and 20 cm respectively. The amount of trees belonging to each diameter class for each of the three analyzed plots is given in Table 1.

4. Results

4.1. Dataset comparison

The analyzed sensors and acquisition pattern deliver largely different point clouds of varying characteristics. Table 4 show the most important acquisition information as well as the overall point density as averaged over all three analyzed plots. The two TLS instruments deliver the highest point densities, whereas the difference between the FARO and Leica TLS point clouds can be accounted on the one hand to the difference between leaf-on and leaf-off acquisitions, but on the other hand also to the increased scan overlap due to a denser scanning pattern chosen with the Leica BLK360 TLS. The GoPro photogrammetry and ZebRevo PLS acquisition deliver the next highest point densities. As shown in Fig. 4, the acquisitions are limited in their vertical range, where the GoPro acquisitions can deliver canopy information up to maximum 10 m and the ZebRevo PLS up to 20 m above ground. The difference between the two airborne acquisitions can be mainly accounted to the difference in season, sensor and acquisition pattern, delivering an overall higher point density for the VUX1 UAVLS instrument (leaf-off) throughout the entire vertical extent.

4.2. Automatic tree detection

The under leaf-off conditions acquired FARO TLS point cloud showed the highest TDR of all tested sensors in all three analyzed plots, with a TDR of up to 94.6% for the plot FP05, when only trees with a DBH ≥ 20 cm are considered. The leaf-on acquisitions of the Leica TLS and ZebRevo PLS instrument show a similar TDR of around 80% in FP05, irrespective of DBH class, and a range between 45 and 80% in FP07, depending on the DBH class analyzed. In FP08, the ZebRevo PLS performed worse compared to the Leica TLS instrument with a TDR of 27.8% versus 50.8% for trees with a DBH ≥ 7 cm. This could be partially explained by the denser understory present in FP08 in combination with many smaller trees just at the DBH threshold of 7 cm and the increased noise level in the ZebRevo PLS dataset. The still lower TDR performance of the ZebRevo PLS also at larger DBH classes can be explained by the fact, that many larger trees were surrounded by denser understorey vegetation, making the detection of the trunks in combination with a higher noise level more difficult. Also for the above canopy LiDAR acquisition, the acquisitions under leaf-off conditions (VUX) show a better tree detection rate than the leaf-on miniVUX acquisition (TDR of 34.8–72.2% vs. 8.7–32.2% at 7 cm DBH threshold). The miniVUX UAVLS acquisition struggled with penetrating through the canopy, resulting in large occlusion effects in the middle- and understorey, leading to many incomplete representations of tree trunks. Of course, also difference in the level of accuracy and noise of the two UAV systems can be an explanation for this large difference in TDR. Considering the lower coverage of the GoPro acquisition due to the chosen circular acquisition path with only 85%, 68%, and 82% of the interpretation area for FP05, FP07, and FP08 respectively, the TDR of 45.6%, 29.8% and 39% at 7 cm DBH threshold shows quite good potential for this low-cost solution. The coverage was estimated based on the coverage of the digital terrain model (DTM) extracted from the GoPro acquisition in comparison with the FARO TLS DTM, which covered the entire 50 m × 50 m plots. The respective DTMs were extracted based on the lowest point of the respective point clouds on a grid with grid size of 1 m using the *lasgrid* function of LASTools (Isenburg, 2015).

Fig. 5(a) shows the TDR for all tested sensors on the three plots. In general one can observe that the TDR under leaf-off conditions tends to be higher. The difference between leaf-on and leaf-off for the FARO and Leica TLS acquisitions for plots FP07 and FP08 is smaller than for FP05. The complexity of the plots, especially in terms of understorey vegetation coverage, has a big influence on the TDR, resulting in higher TDR for the simpler FP05 plot over all three DBH classes, compared to the more complex plots FP07 and FP08, where the difference between DBH classes is also larger.

The complexity of the analyzed plots also shows a big influence on the number of falsely detected trees, as seen in Fig. 5(b). The more complex plots FP07 and FP08 show more falsely detected trees over nearly all instruments (exception: GoPro for FP07) than on FP05. The lowest number of falsely detected trees occur with the ZebRevo PLS system, whereas the highest number of falsely detected trees was found with the above canopy acquisitions of the VUX and miniVUX systems. Especially in the more complex plots FP07 and FP08 many shrub and understorey vegetation clusters were detected as trees, resulting in many falsely detected trees.

In terms of positional accuracy of the detected trees, the FARO TLS system showed highest accuracy with an average distance between detected and reference tree positions of 6 cm over all analyzed trees, followed by ZebRevo PLS with 8.9 cm average displacement. Leica TLS and the GoPro system showed similar performance with 10.1 and 10.9 cm respectively. Largest displacements were encountered with the drone based systems with 22.9 and 20.7 cm for the VUX and miniVUX system respectively.

4.3. Automatic DBH extraction

The FARO TLS acquired leaf-off dataset shows the lowest RMSE of the extracted DBH with an RMSE of 1.6, 1.6 and 1.7 cm for a lower DBH threshold of 7, 12, and 20 cm respectively (relative RMSE of 2.6, 3.0, 3.3% respectively) for plot FP05 as shown in Fig. 6. Also here, the RMSE of the extracted DBH is dependent on the complexity of the plot, as the RMSE increases compared to FP05 when we look at FP07 and FP08. Both UAV systems show the largest RMSE, where the miniVUX system show larger RMSE compared to the VUX system. Noteworthy is the RMSE achieved from the GoPro camera, which is on par or even better than the ground-based LiDAR systems (for FP07 and FP08). This comparison has to be taken with a grain of salt as the amount of trees where a DBH could be extracted is different between the GoPro and LiDAR acquisitions, due to the limited coverage of the GoPro acquisition. The ZebRevo PLS device shows comparable or even

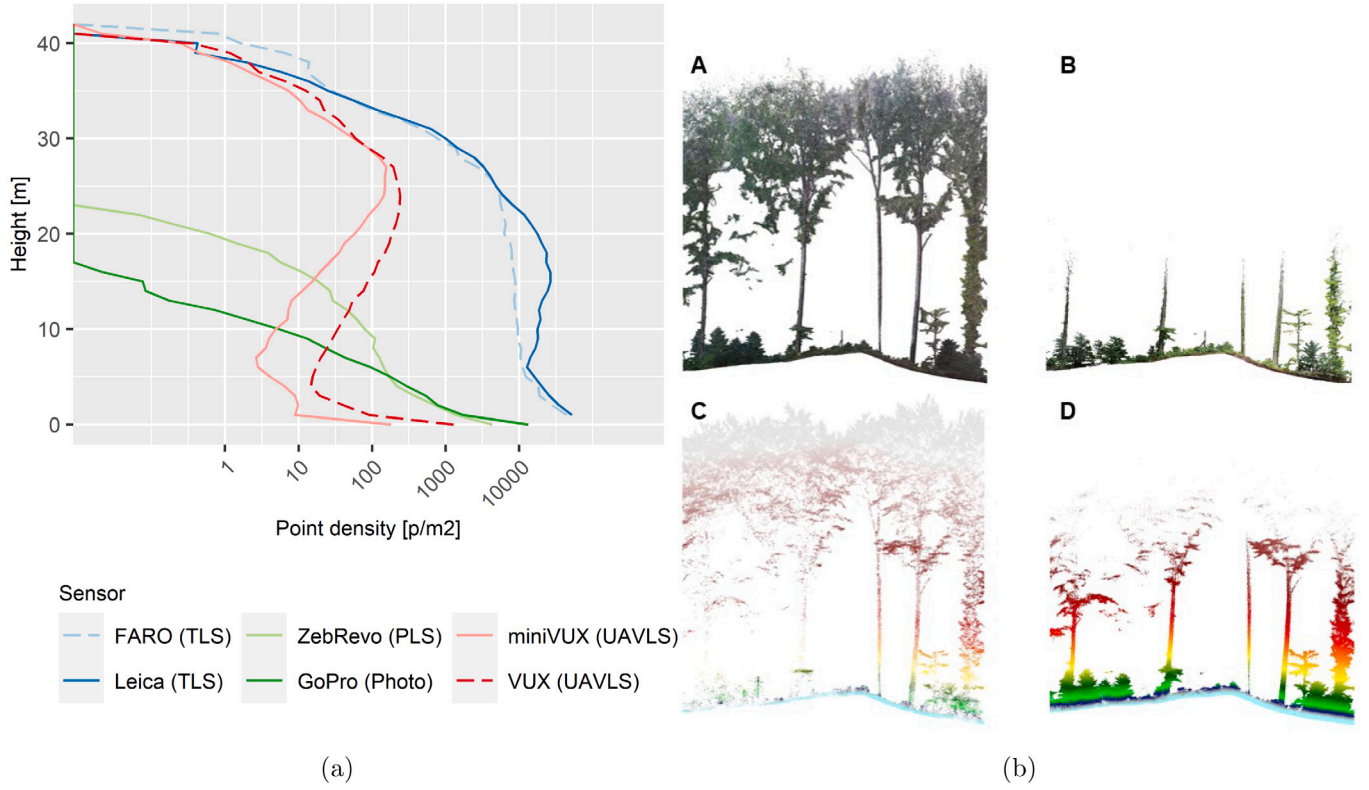

Fig. 4. Vertical point density distribution for the analyzed sensors for plot FP05 (Fig. 4(a)) with average point density per 1 m height slice. Acquisitions under leaf-off conditions are shown as dashed lines, acquisitions under leaf-on conditions are shown in solid lines. For ground point densities see Table 4. Fig. 4(b) shows a slice (depth = 5 m) through acquired point clouds for Leica BLK360 (TLS) (A), GoPro (Photogrammetry) (B), miniVUX2 (UAVLS) (C), and ZebRevo (PLS) (D). (A) and (B) are colored based on RGB camera information, (C) and (D) are colored according to height above ground. (For interpretation of the references to color in this figure legend, the reader is referred to the web version of this article.)

Table 4
Acquisition and point density information for the different acquired point clouds. Ground point densities is the density of all points within a layer of 10 cm above ground. The average over all three analyzed plots are given. If not further stated, time information are given per plot (50 m × 50 m).

	Acquisition date	Acquisition pattern	Acquisition time	Point density [pts/m2]	Ground Point density [pts/m2]
FARO (TLS)	January 2020 (Leaf-Off)	Regular grid $\Delta d \approx 10$ m	6 days (for 1 ha)	869'862	368'723
Leica BLK360 (TLS)	September 2020 (Leaf-On)	Regular grid $\Delta d \approx 5$ m	6 h	1'203'548	211'796
Riegl VUX1 (UAVLS)	March 2020 (Leaf-Off)	Regular grid	≈2 h (for 52 ha)	4'372	884
Riegl miniVUX2 (UAVLS)	September 2020 (Leaf-On)	Regular grid	20 min (for 1 ha)	1'888	82
ZebRevo (PLS)	October 2020 (Leaf-On)	Snake pattern	≈15 min	15'777	3'275
GoPro Hero8 Black (12MP)	September 2020 (Leaf-On)	Circular pattern	≈15 min	29'523	16'845

better results compared to the Leica TLS acquisitions. Only for plot FP08, the ZebRevo PLS device performed worse compared to the Leica TLS instrument, which could be explained by the many small trees close to the 7 cm DBH threshold, where the noise level of the ZebRevo PLS device could be a limitation.

Figs. 7 and 8 show the DBH extraction performance compared to the caliper reference measurements for each ground-based and above canopy sensors respectively. The scatter plots are colored corresponding their plot number. The shaded area corresponds to the 0.95 confidence interval. All ground-based acquisitions show a very good correspondence to the reference measurements with an R^2 of 0.96 and higher, except for the GoPro acquisition at plot FP05 with an R^2 of 0.84. In general, a slight overestimation of DBH for smaller trees and a slight underestimation for larger trees can be seen for all sensors in all plots. Also for this analysis, the leaf-off FARO TLS acquisition show the best performance with R^2 ranging from 0.973 to 0.983. Interestingly, despite the lower accuracy and higher noise level of the ZebRevo PLS acquisitions, it performed equally or better than the Leica TLS system under equal plot conditions (also shown in Fig. 6).

The R^2 for drone based acquisitions are expectantly lower at 0.904 to 0.918 and 0.702 to 0.913 for the VUX and miniVUX acquisition respectively, depending on the analyzed plot. Due to increased occlusion in the miniVUX acquisition, the amount of detected trees as well as the accuracy of the extracted DBH is significantly lower than for all other analyzed systems (see also Fig. 5).

A per-plot summary of tree detection, tree position accuracy and DBH extraction performance is given in Tables A.6, A.7, and A.8 in the Appendix A. Furthermore, a spatial visualization on tree detection performance and DBH extraction for all tested sensors for all three plots is given in the Supplementary Materials.

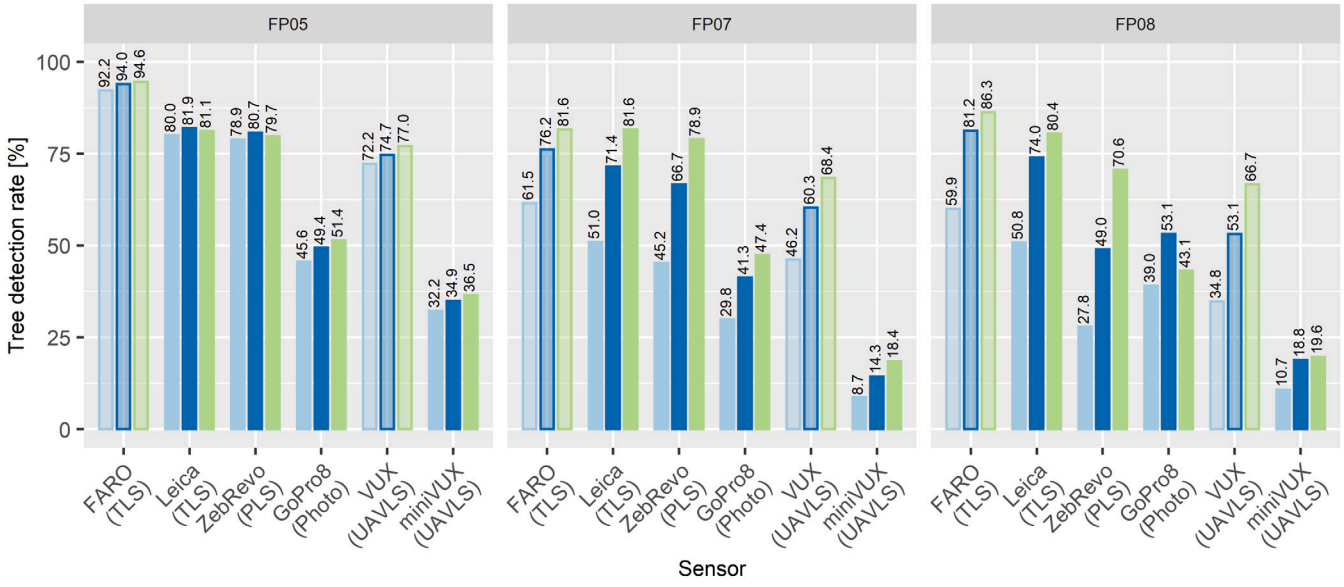

(a)

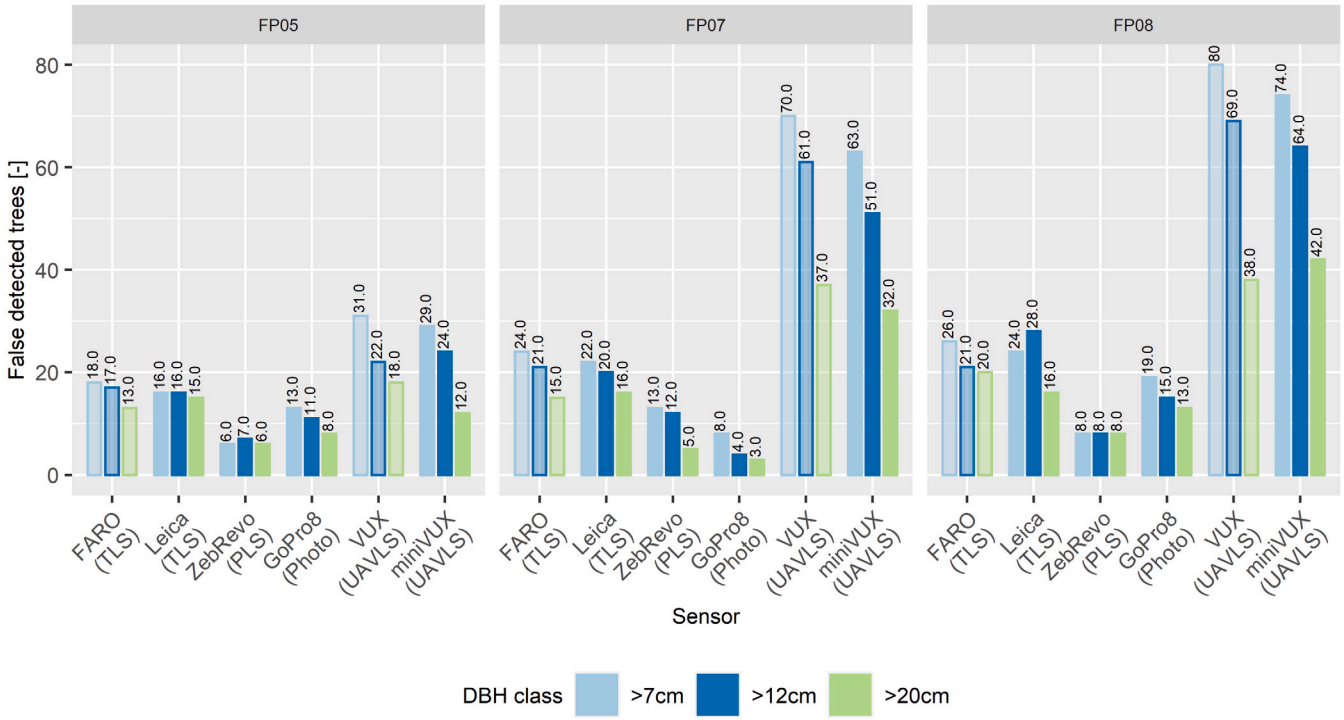

(b)

Fig. 5. Tree detection rate 5(a) and number of falsely detected trees 5(b) for the three plots and six tested instruments, split into three DBH classes of 7 cm and higher, 12 cm and higher and 20 cm and higher Bars for acquisitions under leaf-off conditions are marked with transparent fill FARO (TLS) and VUX (UAVLS).

5. Discussion

5.1. Tree detection performance

5.1.1. Ground-based LiDAR devices

Results showed that TLS acquisitions under leaf-off conditions achieved the highest tree detection rate and most accurate DBH retrieval of the compared devices. Presence of foliage greatly impacts TDR as well as DBH retrieval. This becomes especially visible when we compare the performance of the FARO and Leica TLS acquisitions, as both datasets are comparable in terms of resolution, noise level, point density, and point density distribution (see Section 4.1). The differences in these metrics can be mainly explained by the presence of foliage material. TDR of the ZebRevo PLS system is comparable to the Leica TLS acquisition. However, fewer falsely detected trees were found in the ZebRevo PLS dataset than in the Leica TLS point cloud

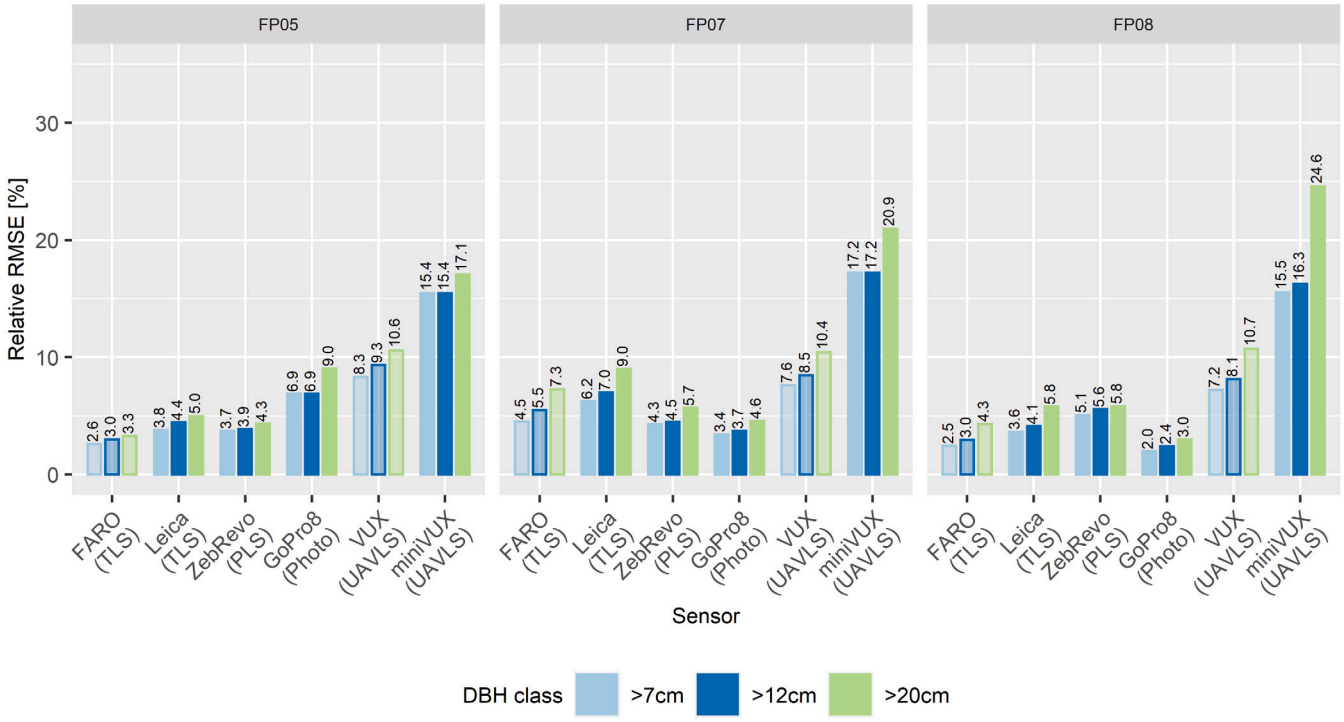

Fig. 6. Relative RMSE of extracted DBH using the RANSAC cylinder fitting approach with applied DBH improvement. Bars for acquisitions under leaf-off conditions are marked with transparent fill FARO (TLS) and VUX (UAVLS).

(see Fig. 5(b)). The fewer amount of falsely detected trees is probably due to the tree mapping approach used in this study. Especially shrubs and denser understorey vegetation can cause a large amount of false positives. Regarding the much faster acquisition time of just 15–30 min for the ZebRevo PLS data versus up to 6 h for the Leica TLS, the handheld PLS system definitely shows big potential towards an operational implementation within a NFI framework. Yet, the chosen TLS scanning setup, with a focus on a complete coverage of the entire forest plot with minimal occlusion, resulted in many scan positions and an increased scanning time. A reduced scanning setup, focusing on acquisition time reduction could make the use of TLS for inventory purposes more operational. However, such a scanning setup adaptation will come at a cost of increased occlusion and hence also a worse tree detection and DBH extraction performance. Abegg et al. (2017) analyzed different TLS scanning setups and its influence on occlusion in relation to forest stand complexity, suggesting optimal scanning setups for increasing the visibility within a stand. Their simulation study also suggest that the highest overall visibility of the stand will be achieved with an evenly distributed scanning setup as performed also in this study.

A significant amount of time for TLS campaigns can be accounted to the setup of artificial targets for the coregistration of individual scan positions. For this reason we wanted to test out the automatic coregistration capabilities of the Leica BLK360 TLS instrument. Unfortunately, the automatic alignment of the scans did fail often in the complex forest environments, why most scans had to be aligned manually during post-processing, counteracting the time gained by not setting up targets. Newer generation of TLS devices including an IMU (e.g. Riegl VZ400i) or SLAM based approaches (e.g. Leica RTC360) for scan coregistration could help in this regard also in more complex environments.

Unfortunately, the maximum range of the ZebRevo PLS of 30 m (manufacturer information) is a largely limiting factor in this regard, as crown information or tree height cannot be retrieved from this data. The successor device GeoSLAM ZebHorizon with a maximum range of 100 m could be a better solution in order to improve the applicability of this type of devices (Gollob et al., 2020). A possible explanation for the good performance of the ZebRevo PLS could be the reduced occlusion in the lower canopy, due to the dense acquisition pattern (see Fig. 2). The acquisition pattern with a PLS device is substantial in this regard and can be a major influence on the performance of the device as also reported by Mokroš et al. (2021), Perugia et al. (2019). Mokroš et al. (2021) stated, that a very dense acquisition can even cause problems for the SLAM based system, resulting in drifts within the point cloud. Forest environments are in general difficult for such SLAM based techniques as only few clearly defined geometric objects are present that can be used by the SLAM approach to align the point clouds. We further observed that the data acquisition with the ZebRevo PLS should not exceed 15 min as this would promote a drift within the trajectory. We showed in this study that also complex plots with a high stem density and dense understorey vegetation can be assessed using the ZebRevo PLS instrument, although at a reduced performance for lower DBH thresholds (7 cm). The successor device GeoSLAM ZebHorizon is reported to perform very well with a tree detection rate of more than 95% at a very low DBH threshold of 5 cm (Gollob et al., 2020). However, these results were achieved under leaf-off conditions, largely reducing the effect of understorey vegetation. TDR for the tested PLS system are comparable to previously published work, where tree detection rates ranged between 57 and 100% (Balenović et al., 2020b). The comparison of these results is difficult as different devices, used with different acquisition patterns and different tree detection approaches were used. As stated by Mokroš et al. (2021) and Balenović et al. (2020b), a thorough analysis of the best acquisition pattern to use has to be performed, possibly resulting in a protocol to guide data acquisition and to further make results more comparable. Similarly, an automatic and robust point cloud segmentation algorithm to detect trees within point clouds of different sources acquired over plots of varying complexity should be pursued (see also Section 5.2).

All point clouds except for the UAVLS acquisitions were absolutely georeferenced by alignment with the absolutely referenced FARO TLS point cloud (see Section 2.2). For a successful inclusion of a specific close-range device in forest inventories, a georeferencing pipeline independent of additional reference point clouds is needed. Some mobile

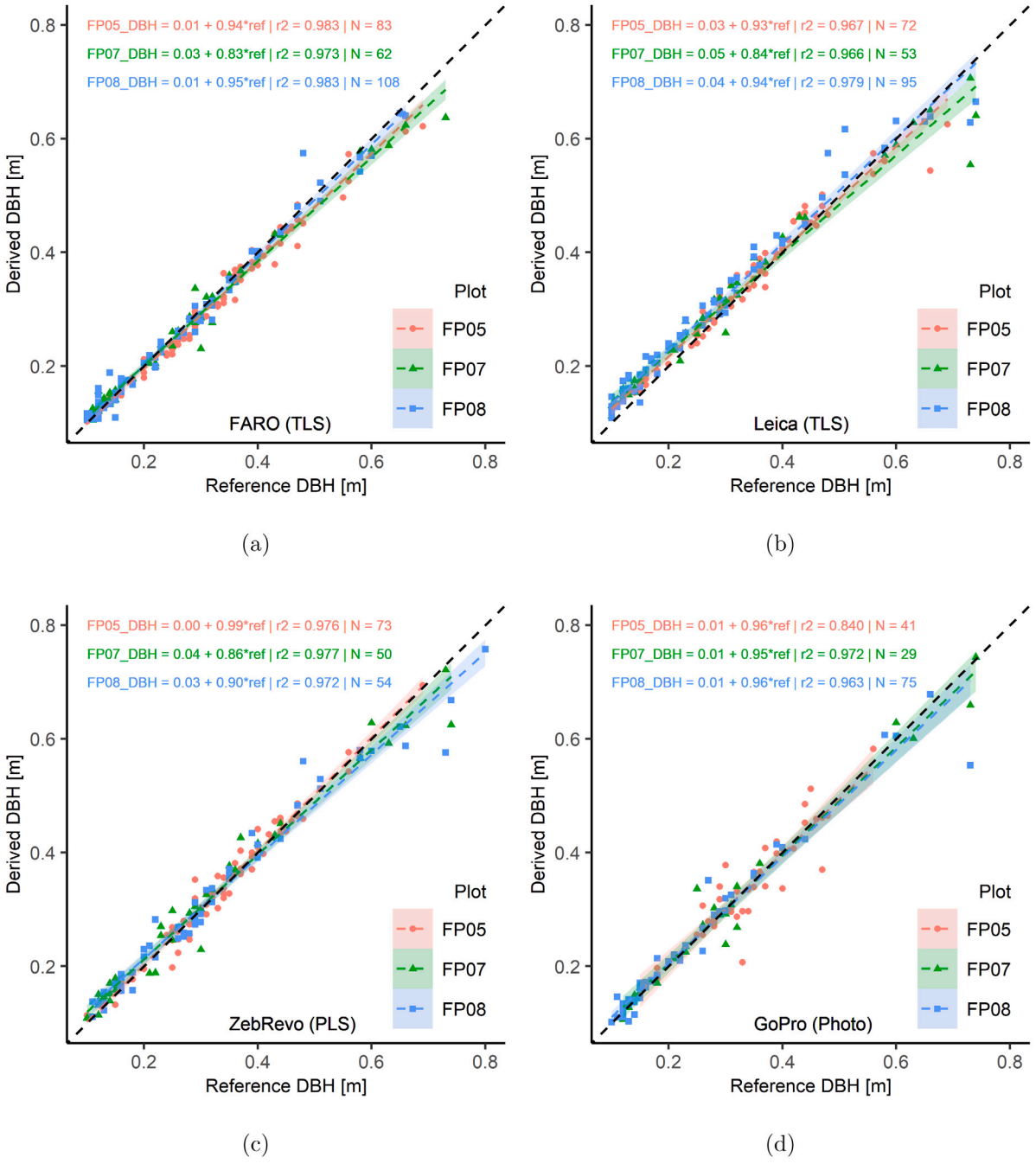

Fig. 7. Derived DBH from on ground sensors versus reference DBH measurements using a caliper. DBH derivation from FARO measurements 7(a), from Leica measurements 7(b), from ZebRevo measurements 7(c), and from GoPro acquired point clouds 7(d). Points and fitted line are colored according to the plot number. Shaded area corresponds to the 0.95 confidence interval. Lower DBH threshold is at 7 cm. (For interpretation of the references to color in this figure legend, the reader is referred to the web version of this article.)

laser scanning devices include already a precise GNSS module (e.g. the GreenValley LiBackPack DGC50). However, accurate positional information within forested environments can be a challenge to acquire. An alternative could be the alignment based on positional information of detectable features within the point clouds. For example, tree positions acquired during traditional field inventory work could be used for a rough point cloud orientation.

5.1.2. *Terrestrial photogrammetry*

While studies on the performance of TLS and PLS systems are numerous, only a few studies analyzed the potential of terrestrial photogrammetry to acquire forest inventory parameters such as DBH and tree positions in natural forests at plot scale (e.g. Liang et al., 2014b, 2015; Panagiotidis et al., 2016; Mikita et al., 2016; Mokroš et al., 2018; Liu et al., 2018; Piermattei et al., 2019). Most of these studies used a single digital SLR camera acquiring multiple images in a stop-and-go movement. As the image acquisition happens while standing still, distortion effects due to movements can be reduced, at the expense of an increased acquisition time. Additionally, the challenging lighting conditions found in natural forests can make the setup of the camera difficult, which can have effects on the quality of the derived point cloud as well as on the success of the point cloud creation. In this study we tried to find a low-cost solution that is very easy to use, without the need for an informed camera setup. Action cameras such as the

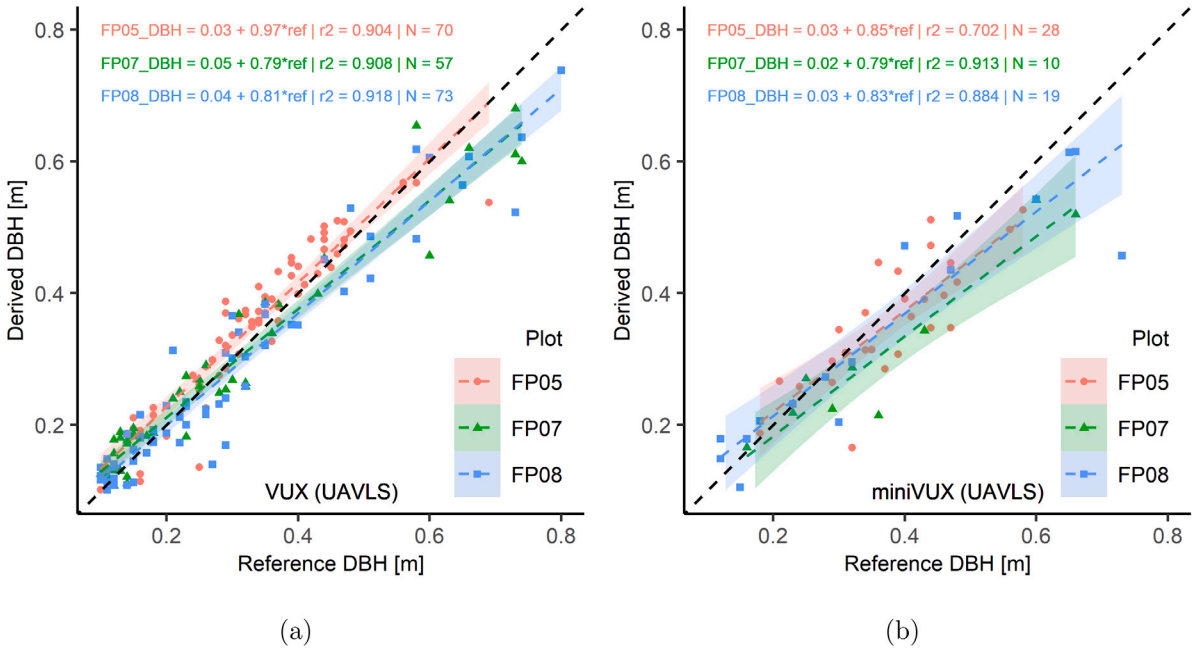

Fig. 8. Derived DBH from above canopy sensors versus reference DBH measurements using a caliper. DBH derivation from VUX acquisition 8(a), and DBH derivation from miniVUX acquisition 8(b). Points and fitted line are colored according to the plot number. Shaded area corresponds to the 0.95 confidence interval. Lower DBH threshold is at 7 cm. (For interpretation of the references to color in this figure legend, the reader is referred to the web version of this article.)

Table A.5
Point cloud filtering and processing options for ground-based (FARO, Leica BLK360, ZebRevo, and GoPro) and above canopy (VUX and miniVUX) sensors for all 3 plots. If no further options for the used functions are declared, default options of the functions are used. Stated functions are implemented in the TreeLS R-Package. Statistical Outlier Removal (SOR) function is implemented in the lidR R-Package. For further explanation of the used functions, please refer to the function descriptions or to de Conto et al. (2017) for TreeLS and Roussel et al. (2020) for lidR functions.

	Filtering	Tree mapping	Stem filtering	Position & DBH extraction
Ground based sensors	1 < Z < 3 m Verticality > 0.8 SOR (k = 6, m = 1)	function: map.eigen.knn options: max_curvature=0.1, max_verticality=10, max_mean_dist=0.1, max_d=0.8, min_h=1, max_h=3	function: stemPoints options: method = stm.hough()	function: tlsInventory options: dh=1.3, dw=1, dmethod=shapeFit shape='cylinder', algorithm='ransac', n=20, n_best=20
Above canopy sensors	1 < Z < 7 m Verticality > 0.8 SOR (k = 6, m = 1)	function: map.eigen.knn options: max_curvature=0.1, max_verticality=10, max_mean_dist=0.3, max_d=0.8, min_h=, max_h=7	function: stemPoints options: method=stm.hough()	function: tlsInventory options: dh=1.3, dw=5, dmethod=shapeFit, shape='cylinder', algorithm='ransac', n=20, n_best=20

Table A.6
Tree detection and DBH extraction performance for plot FP05 with lower DBH threshold of 7 cm. FDT corresponds to the number of falsely detected trees, TDR is the tree detection rate and avg. displ. corresponds to the average distance between reference tree position and detected tree for the plot in question. RMSE and rRMSE corresponds to the absolute and relative (in %) RMSE of the extracted DBH. Tree position and DBH was extracted using the RANSAC algorithm with cylinder fit as implemented in the TreeLS R package (de Conto et al., 2017). The number of reference trees for plot FP05 is 90.

Sensor	# detected	# matched	FDT	TDR	avg. displ.	DBH	
						RMSE	rRMSE [%]
FARO (TLS)	101	83	18	0.922	0.052	0.016	2.6
Leica BLK360 (TLS)	88	72	16	0.8	0.059	0.024	3.79
ZebRevo (PLS)	77	71	6	0.79	0.063	0.024	3.7
VUX (UAVLS)	96	65	31	0.722	0.26	0.045	8.33
miniVUX (UAVLS)	58	29	29	0.322	0.138	0.071	15.43
GoPro (Photo)	54	41	13	0.456	0.094	0.03	6.88

GoPro cameras, are known for their small form factor and ruggedness, as well as their good performance under movement. A gimbal can further improve image quality while acquiring data under movement. This makes this setup very easy to use and especially cheap to acquire. To our knowledge, an action camera such as the GoPro camera has not been used to extract forest inventory relevant parameters on forest plots. Due to the image acquisition pattern as well as due to some patches of very dense understorey vegetation, only a subset of the entire plot area could be covered (coverage of 68%–85%). Nevertheless, a tree detection rate of up to 50% could be achieved with only few

Table A.7
Tree detection and DBH extraction performance for plot FP07 with lower DBH threshold of 7 cm. FDT corresponds to the number of falsely detected trees, TDR is the tree detection rate and avg. displ. corresponds to the average distance between reference tree position and detected tree for the plot in question. RMSE and rRMSE corresponds to the absolute and relative (in %) RMSE of the extracted DBH. Tree position and DBH was extracted using the RANSAC algorithm with cylinder fit as implemented in the TreeLS R package (de Conto et al., 2017). The number of reference trees for plot FP07 is 104.

Sensor	# detected	# matched	FDT	TDR	avg. displ.	DBH	
						RMSE	rRMSE [%]
FARO (TLS)	88	64	24	0.615	0.039	0.037	4.51
Leica BLK360 (TLS)	75	53	22	0.51	0.099	0.048	6.25
ZebRevo (PLS)	60	47	13	0.45	0.082	0.038	4.28
VUX (UAVLS)	118	48	70	0.46	0.23	0.074	7.63
miniVUX (UAVLS)	72	9	63	0.086	0.289	0.087	17.19
GoPro (Photo)	39	31	8	0.298	0.136	0.03	3.42

Table A.8
Tree detection and DBH extraction performance for plot FP08 with lower DBH threshold of 7 cm. FDT corresponds to the number of falsely detected trees, TDR is the tree detection rate and avg. displ. corresponds to the average distance between reference tree position and detected tree for the plot in question. RMSE and rRMSE corresponds to the absolute and relative (in %) RMSE of the extracted DBH. Tree position and DBH was extracted using the RANSAC algorithm with cylinder fit as implemented in the TreeLS R package (de Conto et al., 2017). The number of reference trees for plot FP08 is 187.

Sensor	# detected	# matched	FDT	TDR	avg. displ.	DBH	
						RMSE	rRMSE [%]
FARO (TLS)	138	112	26	0.6	0.079	0.021	2.45
Leica BLK360 (TLS)	119	95	24	0.51	0.134	0.034	3.64
ZebRevo (PLS)	60	52	8	0.28	0.13	0.038	5.07
VUX (UAVLS)	145	65	80	0.35	0.20	0.065	7.23
miniVUX (UAVLS)	94	20	74	0.107	0.269	0.08	15.51
GoPro (Photo)	92	73	19	0.39	0.106	0.014	1.98

falsely detected trees. In terms of DBH extraction, the GoPro acquisition actually performed comparably to the high-tech, ground-based LiDAR systems. For the plots FP07 and FP08, the relative RMSE was actually lowest of all analyzed systems. However, this comparison has to be taken with a grain of salt, as the analyzed trees are not the same, due to the lower coverage of the plot area. The lower RMSE for the GoPro acquisitions could also be partially explained through the fact that trees covered with dense understorey vegetation were also not detected in the dataset and hence were also not included in the DBH analysis. These trees could be potentially measured by the LiDAR systems due to their capability to penetrate through the understorey vegetation.

Even-though the data acquisition for the SfM point cloud data is easy in theory, it is still quite a challenge to find an appropriate acquisition pattern that assures a successful image alignment for any plot conditions. Especially very dense understorey can hinder a successful image alignment. This can be particularly frustrating as the success or failure to align the images can only be assured once the images were processed. Therefore, further studies on appropriate image acquisition patterns for varying plot conditions should be pursued to guide the image acquisition.

We believe, that terrestrial photogrammetry shows large potential as an alternative to often more costly LiDAR solutions, if 3D information of the lower 5 meters of the canopy are of interest. Further studies are needed to analyze the robustness of this approach in varying forest conditions and complexities.

5.1.3. UAV LiDAR devices

The analyzed drone based LiDAR devices showed the lowest TDR in combination with the highest amount of falsely detected trees and highest RMSE for the DBH extraction. This is greatly explained by the observation from above the canopy, resulting in occluded areas in the lower canopy region (Schneider et al., 2019), which greatly affects the tree detection and DBH extraction, especially when tree position was detected at DBH height.

The analysis showed that the season of data acquisition definitely plays a large role for the acquisition of tree metrics from UAV LiDAR data. For tree positional information compatible with on ground measurements and DBH extraction, an acquisition under leaf-off conditions is favorable. The acquisition pattern can largely aid the analysis of the vertical forest structure, as additional observation angles usually tends to decrease occlusion effects (Kükenbrink et al., 2017; Schneider et al., 2019). Additional research should be performed in analyzing additional flight patterns under varying forest conditions to guide future UAVLS campaigns for forestry applications.

Table A.9
Absolute distance between detected and reference tree positions. Tree positions extracted with RANSAC and cylinder fitting with DBH improvement enabled (see Section 3.1). DBH threshold of 7 cm. Units are in meters.

	Average	Median	Stdev
FARO (TLS)	0.06	0.021	0.132
Leica (TLS)	0.101	0.071	0.136
ZebRevo (PLS)	0.089	0.045	0.156
VUX (UAVLS)	0.229	0.206	0.157
miniVUX (UAVLS)	0.207	0.114	0.233
GoPro (Photo)	0.109	0.064	0.155

5.2. Automatic point cloud segmentation

This study does not only highlight differences in the performance of different sensors, as discussed in the previous Section 5.1, but also differences between different plots measured with the same instrument. The three plots analyzed in this study show a gradient in complexity and amount of understorey vegetation present. Even with the gradient in canopy complexity, we did not optimize the point cloud filtering and tree detection approach for the different plots. Results could potentially be improved for individual plots by optimizing the mapping and filtering parameters to the given plot characteristics (e.g. increasing verticality threshold as well as neighborhood in which verticality is calculated for areas with denser understory, selecting a slice through the point clouded located above dense understorey if the canopy structure allows for such a separation, adapting the tree mapping parameters (see Table A.5 in the Appendix A) based on a trial and error approach etc.). This process can be tedious and labor intensive, especially if more plots should be analyzed. In very complex plots, with varying understorey vegetation densities, even an adaptation of the mapping and filtering

parameters within the same plot may be necessary. Currently freely available tools to map tree positions and extract relevant tree metrics, such as the TreeLS R-Package (de Conto et al., 2017), often focus on a specific LiDAR device (TLS or PLS) and are hence also optimized to work with these sensors. Adapting the tools to work with sensors delivering point clouds of different resolution or accuracy can be tedious, time consuming or sometimes even impossible due to restrictions imposed by the sensor's characteristics. This makes a fair comparison between sensors regarding their tree position and metrics extraction performance difficult. A sensor agnostic approach would therefore be of interest, which is also able to handle variations in point cloud quality due to forest plot variations.

6. Conclusion & outlook

In this study we compared and evaluated multiple ground-based and above canopy systems for acquiring 3D point clouds. The comparison was based on the performance to extract NFI relevant tree information (tree position and DBH) in three forest plots of varying tree and undergrowth density. For the ground-based systems, two commonly used TLS systems (FARO Focus 3D and Leica BLK360) and one handheld personal laser scanning (PLS) device (GeoSLAM ZebRevo) were used. Additionally a novel approach using a low-cost action camera (GoPro Hero8 Black) in conjunction with the structure from motion (SfM) methodology was tested and evaluated. For the above canopy vantage point, two UAVLS systems (VUX and miniVUX) were analyzed. Data acquisitions took place under leaf-on and leaf-off conditions. Acquisition time for each plot varied depending on the device used from up to a whole day (TLS), down to 15 min (PLS, GoPro, UAVLS).

Overall, TLS showed the most accurate and robust performance of the tested devices. The high acquisition costs as well as the labor intensive scanning approach, when trying to minimize occlusion, make this device less feasible in a NFI framework. The PLS device has the advantage of a very fast acquisition time, at the cost of lower resolution and accuracy in the point cloud. The results of this study showed, that this does not have a big impact on the performance to detect tree position and extract DBH. The tested PLS device (ZebRevo) therefore shows high potential for the use within a NFI, especially when focusing on forest metrics of the lower strata (up to 15–20 m above ground). With the newer generations of PLS devices (e.g. GeoSLAM ZebHorizon), even a coverage up to the tree top could be possible. Further research on the optimal acquisition pattern for forest plots of varying complexities has to be performed in order to come up with a guideline for robust point cloud acquisitions with these devices. The same goes with the novel approach to use a simple action camera (GoPro). The GoPro acquisition showed high potential to acquire accurate tree positions and DBH information. Tests on more forest plots with varying complexities should be performed to give a conclusive evaluation on the usability of this low-cost and easy-to-use approach within a NFI. The analyzed above canopy LiDAR devices showed the lowest performance in terms of tree detection and DBH extraction of the analyzed systems. Especially under leaf-on conditions, occlusion can greatly hinder the assessment in the lower canopy strata. If detailed assessment of the lower strata is of relevance we would recommend using UAVLS devices mainly under leaf-off conditions. The performance could be improved by adapting the flight and scanning pattern, for which further analysis have to be performed in order to come up with guidelines on best acquisition patterns for given conditions.

Overall, even-though TLS still delivers the most accurate and reliable results, newer mobile approaches such as handheld laser scanning devices or terrestrial photogrammetry show potential for an operational inclusion within the framework of an NFI. Especially their fast data acquisition, while still delivering accurate NFI relevant metrics (tree position, DBH), could make such devices a potentially valuable addition to ongoing national forest inventories.

Funding

This research was conducted within the scientific project "Assessment of the potential of close-range remote sensing to support the Swiss National Forest Inventory" of the Swiss National Forest Inventory. The project was supported by the Swiss Federal Office for the Environment (FOEN).

CRediT authorship contribution statement

Daniel Kükenbrink: Conceptualization, Data curation, Formal analysis, Investigation, Methodology, Validation, Visualization, Writing – original draft, Writing – review & editing. **Mauro Marty:** Conceptualization, Data curation, Formal analysis, Methodology, Writing – original draft, Writing – review & editing. **Ruedi Bösch:** Conceptualization, Data curation, Formal analysis, Methodology, Writing – original draft, Writing – review & editing. **Christian Ginzler:** Conceptualization, Data curation, Formal analysis, Methodology, Project administration, Funding acquisition, Writing – original draft, Writing – review & editing.

Declaration of competing interest

The authors declare that they have no known competing financial interests or personal relationships that could have appeared to influence the work reported in this paper.

Data availability

Data will be made available on request.

Acknowledgment

The authors would like to thank Christoph Düggelin and Fabricio Gioldi for their support during the field survey and fruitful discussions. We are also grateful to Natalia Rehush, Meinrad Abegg, and Christoph Fischer for the frequent and fruitful discussions. We thank the Swiss NFI for the support in acquiring and providing field data. We would also like to thank the two anonymous reviewers for their valuable comments.

Appendix A

A.1. Tree detection workflow

See Table A.5.

A.2. Tree detection and DBH extraction performance per plot

See Tables A.5–A.8.

A.3. Tree displacement

See Table A.9.

Appendix B. Supplementary data

Supplementary material related to this article can be found online at https://doi.org/10.1016/j.jag.2022.102999.

References

Abegg, M., Kükenbrink, D., Zell, J., Schaepman, M.E., Morsdorf, F., 2017. Terrestrial laser scanning for forest inventories-tree diameter distribution and scanner location impact on occlusion. Forests 8 (6), 1–29. http://dx.doi.org/10.3390/f8060184.

Balenović, I., Liang, X., Jurjević, L., Hyyppä, J., Seletković, A., Kukko, A., 2020a. Hand-held personal laser scanning – current status and perspectives for forest inventory application. Croat. J. For. Eng. 42 (1), 165–183. http://dx.doi.org/10.5552/crojfe.2021.858.

Balenović, I., Liang, X., Jurjević, L., Hyyppä, J., Seletković, A., Kukko, A., 2020b. Hand-held personal laser scanning – current status and perspectives for forest inventory application. Croat. J. For. Eng. 42 (1), 165–183. http://dx.doi.org/10.5552/crojfe.2021.858.

Bruggisser, M., Hollaus, M., Kükenbrink, D., Pfeifer, N., 2019. Comparison of forest structure metrics derived from UAV LIDAR and ALS DATA. In: ISPRS Annals of the Photogrammetry, Remote Sensing and Spatial Information Sciences, Vol. 4. (2/W5), pp. 325–332. http://dx.doi.org/10.5194/isprs-annals-IV-2-W5-325-2019.

Cabo, C., Del Pozo, S., Rodríguez-Gonzálvez, P., Ordóñez, C., González-Aguilera, D., 2018. Comparing terrestrial laser scanning (TLS) and wearable laser scanning (WLS) for individual tree modeling at plot level. Remote Sens. 10 (4), http://dx.doi.org/10.3390/rs10040540.

Čerňava, J., Mokroš, M., Tuček, J., Antal, M., Slatkovská, Z., 2019. Processing chain for estimation of tree diameter from GNSS-IMU-based mobile laser scanning data. Remote Sens. 11 (6), 615. http://dx.doi.org/10.3390/rs11060615.

de Conto, T., Olofsson, K., Görgens, E.B., Rodriguez, L.C.E., Almeida, G., 2017. Performance of stem denoising and stem modelling algorithms on single tree point clouds from terrestrial laser scanning. Comput. Electron. Agric. 143 (October), 165–176. http://dx.doi.org/10.1016/j.compag.2017.10.019.

Durrant-Whyte, H., Bailey, T., 2006. Simultaneous localization and mapping: Part i. IEEE Robot. Autom. Mag. 13 (2), 99–108. http://dx.doi.org/10.1109/MRA.2006.1638022.

Fischer, C., Traub, B., 2019. Swiss national forest inventory: methods and models of the fourth assessment. In: Fischer, C., Traub, B. (Eds.), Managing Forest Ecosystems. p. 431. http://dx.doi.org/10.1007/978-3-030-19293-8.

Forsman, M., Holmgren, J., Olofsson, K., 2016. Tree stem diameter estimation from mobile laser scanning using line-wise intensity-based clustering. Forests 7 (9), http://dx.doi.org/10.3390/f7090206.

Gollob, C., Ritter, T., Nothdurft, A., 2020. Forest inventory with long range and high-speed personal laser scanning (PLS) and simultaneous localization and mapping (SLAM) technology. Remote Sens. 12 (9), http://dx.doi.org/10.3390/RS12091509.

Heinzel, J., Ginzler, C., 2019. A single-tree processing framework using terrestrial laser scanning data for detecting forest regeneration. Remote Sens. 11 (1), 1–20. http://dx.doi.org/10.3390/rs11010060.

Isenburg, M., 2015. LAStools—Efficient tools for LiDAR processing. URL https://rapidlasso.com/lastools/.

Jaakkola, A., Hyyppä, J., Yu, X., Kukko, A., Kaartinen, H., Liang, X., Hyyppä, H., Wang, Y., 2017. Autonomous collection of forest field reference—The outlook and a first step with UAV laser scanning. Remote Sens. 9 (8), 1–12. http://dx.doi.org/10.3390/rs9080785.

Kükenbrink, D., Schneider, F., Leiterer, R., Schaepman, M., Morsdorf, F., 2017. Quantification of hidden canopy volume of airborne laser scanning data using a voxel traversal algorithm. Remote Sens. Environ. 194, http://dx.doi.org/10.1016/j.rse.2016.10.023.

Kukko, A., Kaartinen, H., Hyyppä, J., Chen, Y., 2012. Multiplatform mobile laser scanning: Usability and performance. Sensors (Switzerland) 12 (9), 11712–11733. http://dx.doi.org/10.3390/s120911712.

Liang, X., Hyyppa, J., Kukko, A., Kaartinen, H., Jaakkola, A., Yu, X., 2014a. The use of a mobile laser scanning system for mapping large forest plots. IEEE Geosci. Remote Sens. Lett. 11 (9), 1504–1508. http://dx.doi.org/10.1109/LGRS.2013.2297418.

Liang, X., Jaakkola, A., Wang, Y., Hyyppä, J., Honkavaara, E., Liu, J., Kaartinen, H., 2014b. The use of a hand-held camera for individual tree 3D mapping in forest sample plots. Remote Sens. 6 (7), 6587–6603. http://dx.doi.org/10.3390/rs6076587.

Liang, X., Kankare, V., Hyyppä, J., Wang, Y., Kukko, A., Haggrén, H., Yu, X., Kaartinen, H., Jaakkola, A., Guan, F., Holopainen, M., Vastaranta, M., 2016. Terrestrial laser scanning in forest inventories. ISPRS J. Photogramm. Remote Sens. 115, 63–77. http://dx.doi.org/10.1016/j.isprsjprs.2016.01.006.

Liang, X., Kukko, A., Hyyppä, J., Lehtomäki, M., Pyörälä, J., Yu, X., Kaartinen, H., Jaakkola, A., Wang, Y., 2018. In-situ measurements from mobile platforms: An emerging approach to address the old challenges associated with forest inventories. ISPRS J. Photogramm. Remote Sens. 143 (January), 97–107. http://dx.doi.org/10.1016/j.isprsjprs.2018.04.019.

Liang, X., Wang, Y., Jaakkola, A., Kukko, A., Kaartinen, H., Hyyppä, J., Honkavaara, E., Liu, J., 2015. Forest data collection using terrestrial image-based point clouds from a handheld camera compared to terrestrial and personal laser scanning. IEEE Trans. Geosci. Remote Sens. 53 (9), 5117–5132. http://dx.doi.org/10.1109/TGRS.2015.2417316.

Liang, X., Wang, Y., Pyörälä, J., Lehtomäki, M., Yu, X., Kaartinen, H., Kukko, A., Honkavaara, E., Issaoui, A.E., Nevalainen, O., Vaaja, M., Virtanen, J.P., Katoh, M., Deng, S., 2019. Forest in situ observations using unmanned aerial vehicle as an alternative of terrestrial measurements. For. Ecosyst. 6 (1), http://dx.doi.org/10.1186/s40663-019-0173-3.

Liu, J., Feng, Z., Yang, L., Mannan, A., Khan, T.U., Zhao, Z., Cheng, Z., 2018. Extraction of sample plot parameters from 3D point cloud reconstruction based on combined RTK and CCD continuous photography. Remote Sens. 10 (8), http://dx.doi.org/10.3390/RS10081299.

Mikita, T., Janata, P., Surový, P., 2016. Forest stand inventory based on combined aerial and terrestrial close-range photogrammetry. Forests 7 (8), 1–14. http://dx.doi.org/10.3390/f7080165.

Mokroš, M., Liang, X., Surový, P., Valent, P., Čerňava, J., Chudý, F., Tunák, D., Saloň, I., Merganič, J., 2018. Evaluation of close-range photogrammetry image collection methods for estimating tree diameters. ISPRS Int. J. Geo-Inf. 7 (3), http://dx.doi.org/10.3390/ijgi7030093.

Mokroš, M., Mikita, T., Singh, A., Tomaštík, J., Chudá, J., Wężyk, P., Kuželka, K., Surový, P., Klimánek, M., Zięba-Kulawik, K., Bobrowski, R., Liang, X., 2021. Novel low-cost mobile mapping systems for forest inventories as terrestrial laser scanning alternatives. Int. J. Appl. Earth Obs. Geoinf. 104, 102512. http://dx.doi.org/10.1016/j.jag.2021.102512.

Morsdorf, F., Kükenbrink, D., Schneider, F.D., Abegg, M., Schaepman, M.E., 2018. Close-range laser scanning in forests: towards physically based semantics across scales. Interface Focus 8 (2), 20170046. http://dx.doi.org/10.1098/rsfs.2017.0046.

Nocerino, E., Menna, F., Remondino, F., Toschi, I., Rodríguez-Gonzálvez, P., 2017. Investigation of indoor and outdoor performance of two portable mobile mapping systems. In: Videometrics, Range Imaging, and Applications XIV, Vol. 10332. (June 2017), p. 103320I. http://dx.doi.org/10.1117/12.2270761.

Panagiotidis, D., Surový, P., Kuželka, K., 2016. Accuracy of structure from motion models in comparison with terrestrial laser scanner for the analysis of DBH and height influence on error behaviour. J. For. Sci. 62 (8), 357–365. http://dx.doi.org/10.17221/92/2015-JFS.

Perugia, B.D., Giannetti, F., Chirici, G., Travaglini, D., 2019. Influence of scan density on the estimation of single-tree attributes by hand-held mobile laser scanning. Forests 10 (3), 1–13. http://dx.doi.org/10.3390/f10030277.

Piermattei, L., Karel, W., Wang, D., Wieser, M., Mokroš, M., Surový, P., Koreň, M., Tomaštík, J., Pfeifer, N., Hollaus, M., 2019. Terrestrial structure from motion photogrammetry for deriving forest inventory data. Remote Sens. 11 (8), http://dx.doi.org/10.3390/rs11080933.

Rehush, N., Abegg, M., Waser, L.T., Brändli, U.B., 2018. Identifying tree-related microhabitats in TLS point clouds using machine learning. Remote Sens. 10 (11), 1–23. http://dx.doi.org/10.3390/rs10111735.

Roussel, J.R., Auty, D., Coops, N.C., Tompalski, P., Goodbody, T.R., Meador, A.S., Bourdon, J.F., de Boissieu, F., Achim, A., 2020. LidR: An R package for analysis of airborne laser scanning (ALS) data. Remote Sens. Environ. 251, 1–17. http://dx.doi.org/10.1016/j.rse.2020.112061.

Schneider, F.D., Kükenbrink, D., Schaepman, M.E., Schimel, D.S., Morsdorf, F., 2019. Quantifying 3D structure and occlusion in dense tropical and temperate forests using close-range LiDAR. Agricult. Forest Meteorol. 268 (2019b), 249–257. http://dx.doi.org/10.1016/j.agrformet.2019.01.033.

Terryn, L., Calders, K., Bartholomeus, H., Bartolo, R.E., Brede, B., D'Hont, B., Disney, M., Herold, M., Lau, A., Shenkin, A., Whiteside, T.G., Wilkes, P., Verbeeck, H., 2021. Quantifying tropical forest stand structure through terrestrial and UAV laser scanning fusion, vol. 271, no.september 2021. pp. 8281–8284. http://dx.doi.org/10.1109/igarss47720.2021.9553992.

Wieser, M., Mandlburger, G., Hollaus, M., Otepka, J., Glira, P., Pfeifer, N., 2017. A case study of UAS borne laser scanning for measurement of tree stem diameter. Remote Sens. 9 (11), 1–11. http://dx.doi.org/10.3390/rs9111154.

Yrttimaa, T., Saarinen, N., Luoma, V., Tanhuanpää, T., Kankare, V., Liang, X., Hyyppä, J., Holopainen, M., Vastaranta, M., 2019. Detecting and characterizing downed dead wood using terrestrial laser scanning. ISPRS J. Photogramm. Remote Sens. 151, 76–90. http://dx.doi.org/10.1016/j.isprsjprs.2019.03.007.